A Techno-Economic Analysis of Energy Storage Components of Microgrids for Improving Energy Management Strategies

Alla Ndiaye, Fabrice Locment, Alexandre de Bernardinis, Manuela Sechilariu, Eduardo Redondo-Iglesias

energies

MDPI

Article

A Techno-Economic Analysis of Energy Storage Components of Microgrids for Improving Energy Management Strategies

Alla Ndiaye [1], Fabrice Locment [1], Alexandre De Bernardinis [2], Manuela Sechilariu [1,*] and Eduardo Redondo-Iglesias [3]

[1] AVENUES, Centre Pierre Guillaumat, Université de Technologie de Compiègne, 60200 Compiègne, France; alla.ndiaye@univ-lille.fr (A.N.); fabrice.locment@utc.fr (F.L.)
[2] LMOPS, IUT Thionville-Yutz, Université de Lorraine, 54052 Nancy, France; aleandre.de-bernardinis@univ-lorraine.fr
[3] Eco7, AME, Université Gustave Eiffel, 69675 Bron, France; eduardo.redondo@univ-eiffel.fr
* Correspondence: manuela.sechilariu@utc.fr; Tel.: +33-03-44-23-50-27

Abstract: Microgrids are essential elements of the energy transition because they allow optimal use of renewable energy sources (photovoltaic panels, wind turbines) and storage devices (batteries, supercapacitors) by connecting them to consumption poles (e.g., buildings, charging stations of electric vehicles). Lithium-ion batteries and supercapacitors are the main electrical storage devices usually used by microgrids for energy and power transient management. In the present paper, microgrid simulations have been performed. Electrothermal and aging models of storage components are presented. Strategies and scenarios for the batteries are presented either based on the state of charge limitation or hybrid association with supercapacitors. The contribution of this study is to provide a management strategy which considers the aging of storage systems in the real-time management of the microgrid in order to extend their life, while minimizing installation costs. The first approach for a techno-economic study provided in that study enables us to improve the strategies by optimizing the use of the battery. The results obtained in this paper demonstrate the key role of the techno-economic approach and knowledge of the aging processes of storage devices in improving the energy management and global feedback costs of microgrids. The simulation results show that battery life can be improved by 2.2 years. The improvement in battery life leads to a reduction in the total cost of the installation by reducing the cost of the batteries.

Keywords: techno-economic analysis; microgrids; lithium-ion batteries; supercapacitors; aging modelling

Citation: Ndiaye, A.; Locment, F.; De Bernardinis, A.; Sechilariu, M.; Redondo-Iglesias, E. A Techno-Economic Analysis of Energy Storage Components of Microgrids for Improving Energy Management Strategies. *Energies* **2022**, *15*, 1556. https://doi.org/10.3390/en15041556

Academic Editors: Francesco Calise, Neven Duić, Maria da Graça Carvalho, Qiuwang Wang and Poul Alberg Østergaard

Received: 17 January 2022
Accepted: 16 February 2022
Published: 20 February 2022

1. Introduction

The security and reliability of large-scale grids are becoming increasingly problematic due to profound changes in the sector such as market liberalization, increased interconnections, and economic and environmental constraints [1]. One of the solutions to these problems is the decentralization of production sites based on renewable energy. Decentralized power generation will, on the one hand, reduce the investment costs of electricity transmission and distribution. On the other hand, it will facilitate the integration of renewable energies into the public grid via microgrids. The final objective is to achieve optimized local production-consumption controlled in real time by an intelligent electricity network. The microgrid framework provides a means of harnessing diverse energy sources, e.g., photovoltaic (PV) panels, wind turbines, and engines, in a decentralized manner, while reducing the load on the grid by generating power close to the consumer [2]. Microgrid aggregates local power production, consumption, and storage together [3]. Storage systems provide security of supply to the microgrid and address fluctuations of renewable energy sources in the grid (e.g., intermittency and randomness of the power generated by PV) [1]. Lithium-ion batteries and supercapacitors (SCs) are the main electrical storage devices

usually used in microgrids for energy and power transient management. Optimized energy management is a key issue for the deployment of microgrids, which will require specific modelling and management tools. In order to improve or reinforce management strategies, the knowledge of a techno-economic study among different operating cases for the storage components is mandatory. To achieve such techno-economic analysis, accurate models for the electrical storage components are first required. In particular, aging models should bring key indicators on how to optimize the state of health (SoH) of the storage components, predict possible fluctuations, and act to preserve the battery lifetime. For the lithium-ion batteries, combined calendar-cycling aging simulations have been performed. For SCs, calendar aging, as well as a degradation model according to the SoH are investigated. In addition, strategies and scenarios for the batteries are presented either based on state of charge (SOC) limitation or hybrid association with SCs in order to extend their lifetime in a microgrid operation, while in the meantime searching for a method of minimizing the installation costs. The techno-economic study approach provided in this study allows us to improve the classical energy management strategy of microgrids, called strategy 1 in this manuscript, by optimizing the use of the battery. First, results for the real-time management of microgrids is achieved by adapting aging models, outputs of the techno-economic study for the battery, and SCs towards real-time implementation. This article is based on the conference paper [4] that was extended to the electro-thermal models of the batteries and the supercapacitor improving, and therefore, the aging aspect of the hybrid storage.

The rest of the paper is organized as follows: Section 2 presents the studied microgrid. The modelling of the hybrid energy storage system (HESS) elements, composed by a lithium-ion battery and supercapacitors, is presented as well as the PV panels and the connection to the utility grid. Then, the three management strategies used are defined. Section 3 presents the simulation results. A comparison is performed between strategies 1 and 2 in different SOC scenarios. A techno-economic study is conducted in this section. The simulation results in the case of HESS are presented. Finally, Section 4 presents the conclusion and perspectives.

2. Energy Management Strategies in Microgrids

The production of PV energy, like other renewable energy production, is intermittent and its injection into the public grid without any control can lead to increased vulnerabilities of the public grid such as voltage and frequency fluctuations [1,2]. Nevertheless, through energy management system, integrating intermittent renewable energy sources into a microgrid avoids most of these vulnerabilities.

A microgrid grid-connected is able to manage, at different time scales, the power flows according to strategies implemented in order to maximize PV energy use and to minimize the energy cost as well as the negative impact concerning the grid. The management of power flows in real-time is carried out either in a simple way, based on rules such as a simple multi-agent system [5] or those of fuzzy logic [6,7], or algorithmically, based on mathematical optimization approaches carried out with an objective function and constraints. Due to its simplicity and efficiency, in this study the rule-based management strategy is applied.

2.1. Presentation of the Microgrid

Microgrids are essential elements of the energy transition as they allow the optimal use of renewable energy sources (e.g., PV panels, wind turbines) by connecting them to loads (buildings, electric vehicle charging stations) or storage systems (batteries, SCs). There are AC, DC, and hybrid AC/DC microgrid structures depending on the usage of AC or DC common bus for coupling different elements within a microgrid. The microgrid combines local power generation and local consumption and can operate in grid-connected or in islanded operation mode [3]. A microgrid controller allows for the connection to the public grid and provides voltage control, energy and power flow, load sharing, load shedding

during islanding, and considers the constraints of the public grid transmitted through a communication bus [1]. Figure 1 shows the studied DC microgrid.

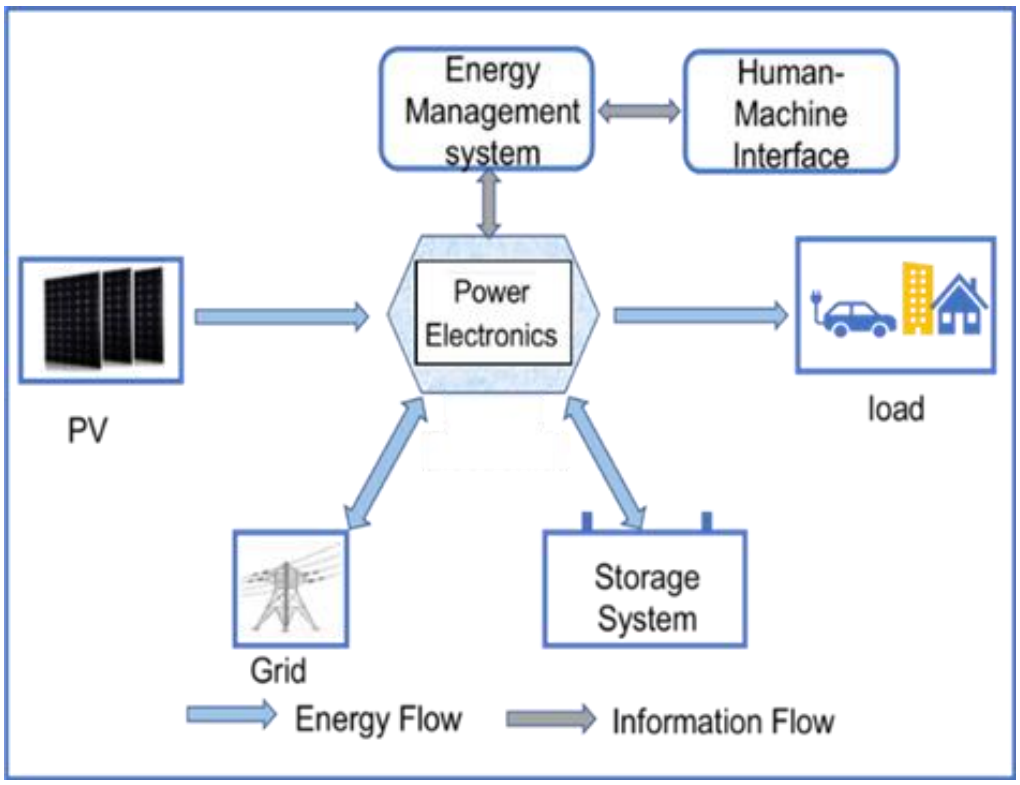

Figure 1. DC microgrid.

2.1.1. Definition of the Hybrid Energy Storage System

Microgrid storage devices are necessary to manage electric grid peak demand, improve reliability and outage mitigation, compensate for intermittent power generation from distributed generation, provide ancillary services specified in an islanded mode of operation, and increase electric grid load factor and utilization via the smart grid [2]. The studied HESS is composed of a lithium-ion battery and SCs. The aging of these storage systems due to various stress factors (e.g., operating temperature, *SOC*, current amplitude) is a major problem in microgrids. As the price per kWh of batteries and SCs is still high today (a few hundred euros depending on the technology), it is essential to extend their life span as much as possible in order to reduce the total cost of the installation. To achieve this objective, better sizing and management are the only solutions. The size of the battery has an impact on the cost of the system and its performances (power and energy availability); optimal energy management can also improve the power and energy availability leading to lower operation costs. Both battery sizing and energy management are strongly related and mutually dependent. This work focuses on the management part.

Lithium-ion batteries: in this section, the electrothermal and aging models of the lithium-ion batteries are presented. The electrical model of the battery is a Thevenin model mainly composed of an OCV (open circuit voltage) source in series with the internal resistance as presented in Figure 2. The dynamic behavior (RC, CPE . . .) is not considered in this model. The cells used for models and simulations are Samsung commercial cells with a nominal capacity of 26 Ah and the chemistry of NMC (Nickel, Manganese, Cobalt) in the positive electrode and graphite in the negative electrode.

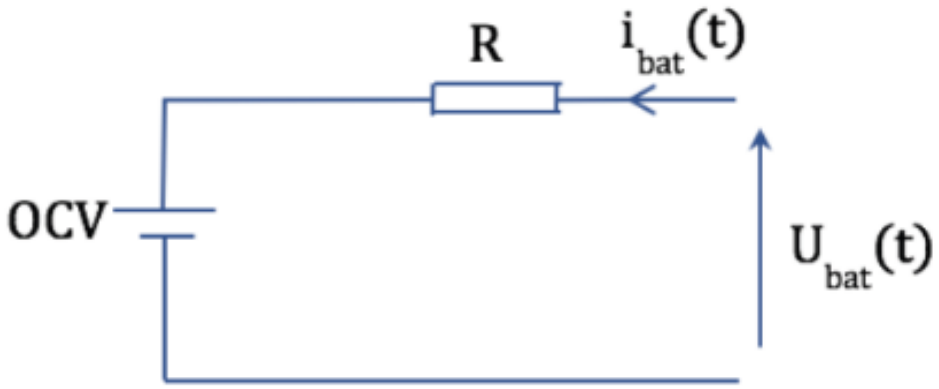

Figure 2. Battery electric model.

The battery thermal model: energy balance for the battery can be written as presented in Equation (1) [8]:

$$C_{Th}\frac{\partial T}{\partial t} = P_{Conv} + P_{Rad} + P_{Heat} \quad (1)$$

where C_{Th} is the heat capacity, and P_{Heat} is the heat generation. The thermal power is assumed to come only from the Joule effect due to the internal resistance of the battery R, as defined in Equation (2). The heat exchange rate is transferred by convection P_{Conv} and radiation P_{Rad}.

$$P_{Heat} = R \times {I_{Bat}}^2 \quad (2)$$

In this work, the thermal model proposed by [9] is employed. This model simplifies Equation (1) into Equation (3). The following assumptions have been considered: the heat capacity of the cell surface is neglected due to the fact that its packaging is very light compared to the core [10]. The heat transfer between the core and the surface (conduction) and between the surface and the air (convection) is represented by the thermal resistance R_{Th} [10]. T_{Bat} is the internal battery temperature, and T_{amb} is the ambient temperature.

$$\frac{dT_{Bat}}{dt} = \frac{T_{amb} - T_{Bat}}{C_{Th} \times R_{Th}} + \frac{P_{Heat}}{C_{Th}} \quad (3)$$

An equivalent thermal circuit is illustrated in Figure 3. P_{Heat} is represented as a source of current, and C_{Th} allows it to store energy like a capacitor. Internal battery temperature T_{Bat} can be determined as well.

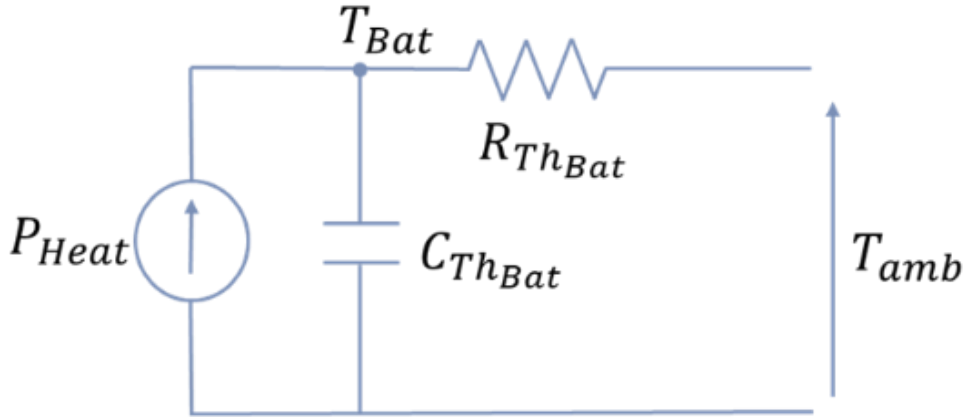

Figure 3. Battery thermal model.

Thermal parameters calibration method: with the battery current in the microgrid being very low (I_{max} = $C/10$), the maximum temperature variation should not exceed 2 °C at a current of $C/5$. In the permanent state, Equation (3) becomes Equation (4). R_{Th} can be

obtained as shown in Equation (5). P_{Heat_max} is determined by Equation (2) with a current value of $C/5$.

$$\frac{T_{amb} - T_{Bat}}{R_{Th}} + P_{Heat\_max} = 0 \tag{4}$$

$$\Rightarrow R_{Th} = \frac{-P_{Heat\_max}}{T_{amb} - T_{Bat}} \tag{5}$$

With the thermal time constant τ_{Th} defined in Equation (6), the thermal capacity can be calculated (7):

$$\tau_{Th} = C_{Th} \times R_{Th} \tag{6}$$

$$C_{Th} = \frac{\tau_{Th}}{R_{Th}} \tag{7}$$

The battery aging model employed is developed in [11]. Based on Eyring's law, this semi-empirical model combines calendar and cycled aging and considers the accumulation of three aging mechanisms (calendar, cold cycling, and hot cycling) in an independent way. More details on the development of the model can be found in [11]. The Eyring law for an "i" cycling aging mechanism is presented in Equation (8).

$$\frac{dq_{loss,i}}{dt} = A_i \times e^{B_i \times SOC} \times e^{\frac{E_{a,i} - C_i \times I}{R \times (T_{bat} - T_r)}} \times I \times \left(\frac{1}{1 + b \times {q_{loss}}^c} \right) \tag{8}$$

where $q_{loss,i}$ is the battery capacity loss (p.u), A_i is the pre-exponential factor (p.u./day), $E_{a,i}$ is the activation energy (J. mol^{-1}), R is the gas constant (J.mol^{-1}.K^{-1}), I is the battery charging current expressed in C-rate, T_{Bat} is the battery temperature (K), B_i is the SOC influence coefficient, and C_i is the current influence coefficient expressed in (h. p.u^{-1}). T_r is the reference temperature where the "i" aging mechanism influence is assumed to be zero (typically $T_r = 0$ K for calendar and hot cycling aging). b and c are unitless model parameters. C-rate is a measure of charging or discharging current, expressed as a ratio of the rated capacity to the time required to fully charge an energy storage system.

To calibrate the model, a current of I_0 = C-rate/12 is chosen. Any cycling at a current less than or equal to this is considered to be calendar aging. Equation (9) gives the variation of the capacity loss of the complete aging model, where $q_{loss-cal}$ is the capacity loss due to calendar aging (10), $q_{loss-cycl-hot}$ is the capacity loss during hot cycling aging (11), and $q_{loss-cycl-cold}$ is the capacity loss during cold cycling aging (12).

$$\frac{dq_{loss}}{dt} = \frac{dq_{loss-cal}}{dt} + \frac{dq_{loss-cycl-hot}}{dt} + \frac{dq_{loss-cycl-cold}}{dt} \tag{9}$$

$$\frac{dq_{loss-cal}}{dt} = \underbrace{A_{cal} \times e^{B \times SOC} \times e^{\frac{-E_{a,cal} + C_{cal} \times I_0}{R \times T_{bat}}} \times \left(\frac{1}{1 + b \times {q_{loss}}^c} \right)}_{calendar\ aging} \tag{10}$$

$$\frac{dq_{loss-cycl-hot}}{dt} = \underbrace{A_c \times e^{B \times SOC} \times e^{\frac{-E_{a,c} + C_c \times I}{R \times T_{bat}}} \times I \times \left(\frac{1}{1 + b \times {q_{loss}}^c} \right)}_{hot\ aging} \tag{11}$$

$$\frac{dq_{loss-cycl-cold}}{dt} = \underbrace{A_f \times e^{B \times SOC} \times e^{\frac{E_{a,f} - C_f \times I}{R \times (T_{bat} - T_r)}} \times I \times \left(\frac{1}{1 + b \times {q_{loss}}^c} \right)}_{cold\ aging} \tag{12}$$

The coupling of the electrothermal and aging model of the battery is presented in Figure 4.

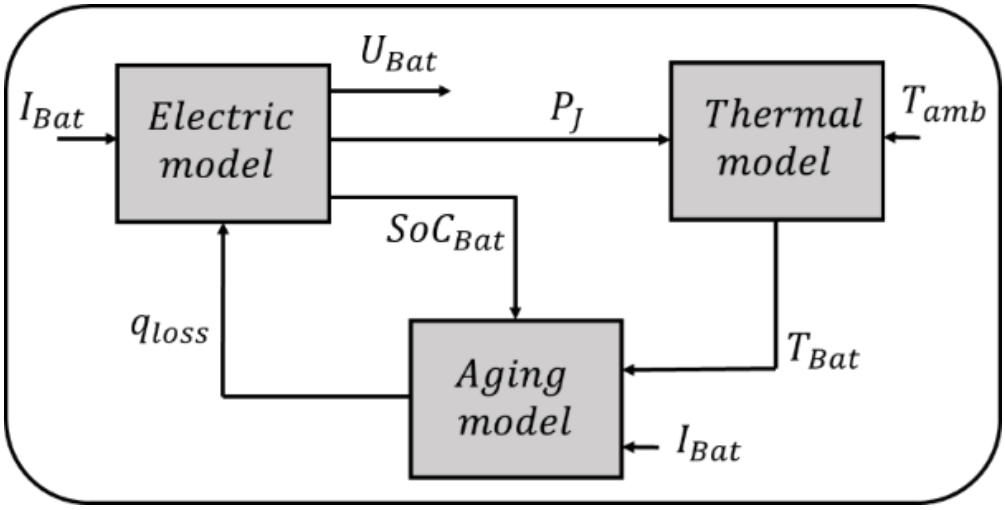

Figure 4. Coupling of the battery electrothermal and aging model.

The Supercapacitors (SCs), also known as Electrochemical Double-Layer Capacitors or ultra-capacitors are less performant than electrochemical batteries in terms of energy density [12]. However, their cycling lifetimes, power densities and operating temperature ranges make them a storage technology used in many applications, whether vehicle or stationary.

In a microgrid involving a HESS composed of batteries and SCs, the SCs allow the lifetime of batteries to be improved. The high-power density of SCs allows transient currents to be absorbed due to the numerous power fluxes of the panels. The management of the power flow for these storage components with the other elements of the microgrid is a key point.

In order to ensure performance over the life of the system, the reliability of SCs has to be quantified through accelerated aging tests and/or the use of aging models. To this purpose, manufacturers and several laboratories have conducted numerous calendar and cycling aging tests.

The electrical model basically consists of Thevenin model with a capacitor C in series with the internal resistance (ESR equivalent series resistance) in the function of time (t), as shown in Figure 5.

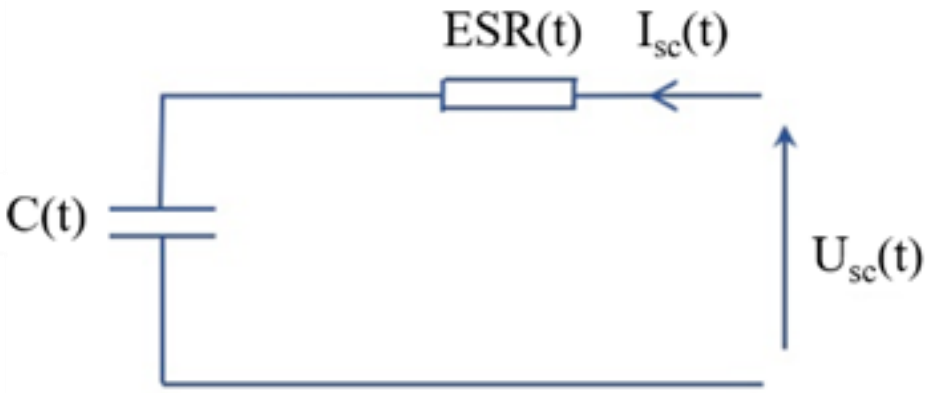

Figure 5. Thevenin electrical model of the SC.

The SCs thermal model: the thermal model of SCs is a standard thermal model in the form of equivalent electrical circuits as presented in [13]. The equivalent electrical circuit is the same as that of the battery (Figure 3). The thermal resistance R_{Th_SC} and the thermal capacity C_{Th_SC} are given in [14].

The SCs aging model: the classical aging model of SC concerns only calendar effects; it is based on the use of Eyring's law, which gives the lifetime [12]. The SoH variation is then given by Equation (13), where θ_0 is the temperature of the case and V the voltage at the terminals of the component. V_0 and θ_0 correspond, respectively, to the voltage and temperature drop required to double the lifetime. t_{Life_Ref} is the reference lifetime in hours, for a reference package temperature θ_{c-Ref} (here, the maximum operating temperature is 65 °C) and a reference voltage V_{Ref} (here, the nominal voltage is 2.7 V).

$$\frac{dSoH}{dt} = \frac{1}{t_{Life-Ref}} \times e^{\ln(2)\frac{\theta_c - \theta_{c-Ref}}{\theta_0}} \times \left[e^{ln(2)\frac{V - V_{Ref}}{V_0}} + K \right] \quad (13)$$

The coefficient K enables us to consider the aging in high temperatures and low voltages [12]. The electrical parameters, the capacitor C and ESR, vary as a function of aging. According to [15], two different phases can be observed during SC aging: an initial burning phase and a linear degradation phase. The model presented in [12] considers only the latter phase considering a linear variation of the capacitance and conductance parameters. Hence, the capacity is equal to 95% of the initial capacity at SoH = 1, as in Equation (14). Equation (15) gives the conductance (i.e., the inverse of the ESR) as a function of SoH. C_0 and ESR_0 are the initial values of C and ESR, respectively (see [12,16] for more details).

$$C = C_0 \times (0.8 + 0.15 \times SoH) \quad (14)$$

$$ESR^{-1} = ESR_0^{-1} \times (0.7 + SoH) \quad (15)$$

2.1.2. Photovoltaic Panel System

The renewable energy source in a microgrid can be PV panels, wind turbines, or both combined. In this study, the renewable energy source considered is based on PV panels. The solar irradiation data used in the simulation are from the PV installation of the Centre Pierre Guillaumat of the Université de Technologie de Compiègne (UTC), which consists of 16 panels in series of 130 W nominal (reference SolarFabrik SF 130/2), as shown in Figure 6. Regarding the experimental platform including the PV installation of the Centre Pierre Guillaumat of UTC, more details can be found in [17].

Figure 6. Photovoltaic installation of the Centre Pierre Guillaumat of UTC [17].

2.1.3. Connection to the Utility Grid

The connection to the public grid is a security element that ensures the safety of the system in case of insufficient power transferable to the load, or excess power [1]. It is assumed that there are no constraints to connect to the grid.

2.2. Development of Control Strategies

The objective of this section is to present the energy management strategies of the microgrid that allow us to extend the battery lifetime and, consequently, to lower the cost of the installation. First, the classical microgrid management strategy is presented. In a second step, two management strategies that allow for the reduction of battery aging are presented. Simulation results are given and discussed.

2.2.1. Strategy 1: Classical Microgrid Energy Management

In this part, the strategy is defined to distribute the extra power between the battery and the public grid considering the *SOC* of the battery. It is assumed that the extra power can be drained to the grid at any time. The extra power, P_{tot}, is the difference between the generated power and the required power to supply the load, as given in Equation (16).

$$P_{tot} = P_c - P_{pv} \tag{16}$$

with P_c the power of the load and P_{pv} the power of the PV panels.

To distribute the extra power between the grid and the battery, a distribution coefficient K_D is defined, as shown in Equations (17) and (18):

$$P_{bat} = K_D \times P_{tot} \tag{17}$$

$$P_G = P_{tot} - P_{bat} = (1 - K_D) \times P_{tot} \tag{18}$$

With: $\begin{cases} K_D = 1 \Rightarrow P_{bat} = P_{tot} \\ K_D = 0 \Rightarrow P_{bat} = 0 \end{cases}$

P_G is utility grid power. The flowchart of this strategy is presented in Figure 7.

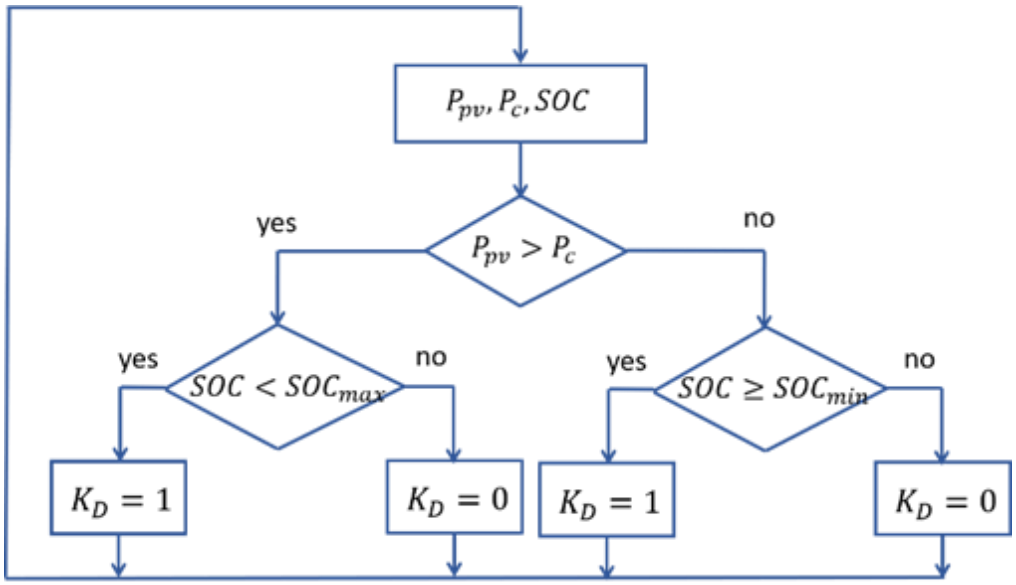

Figure 7. Flowchart of classic management of microgrid.

2.2.2. Control Strategy Considering Battery Aging

Strategy 2: improvement of strategy 1 considering battery aging: the classical strategy is improved. If the generated power is insufficient, the battery is not automatically used to supply the load. The price per kWh from the grid is compared to the price per kWh from the battery. A cost related to the use of the battery is defined. This price includes the cost of the battery, power electronics, cost of installation, step-up transformer, smart-grid communication and controls, grid interconnection to utility [2], the replacement costs, repair and maintenance costs, and the discounted purchase price of the battery [3]. To

simplify the calculations, the price per kWh battery (C_{Bat}) is chosen arbitrarily [3]. The grid kWh price (C_G) varies by time of day:

1. During peak hours, the price per kWh from the grid is higher than the battery's one. The load is supplied from the battery;
2. During off-peak hours, the grid kWh cost is cheaper than the battery's one. Extra power is purchased from the grid. Table 1 shows the prices per kWh for the grid and battery.

Table 1. Price per kWh for grid and battery.

	Grid	Battery
Peak hours	0.7	0.3
Off-peak hours	0.1	0.3

The flowchart for strategy 2 is shown in Figure 8. The influence of the maximum SOC, SOC_{max}, on the battery life is also considered.

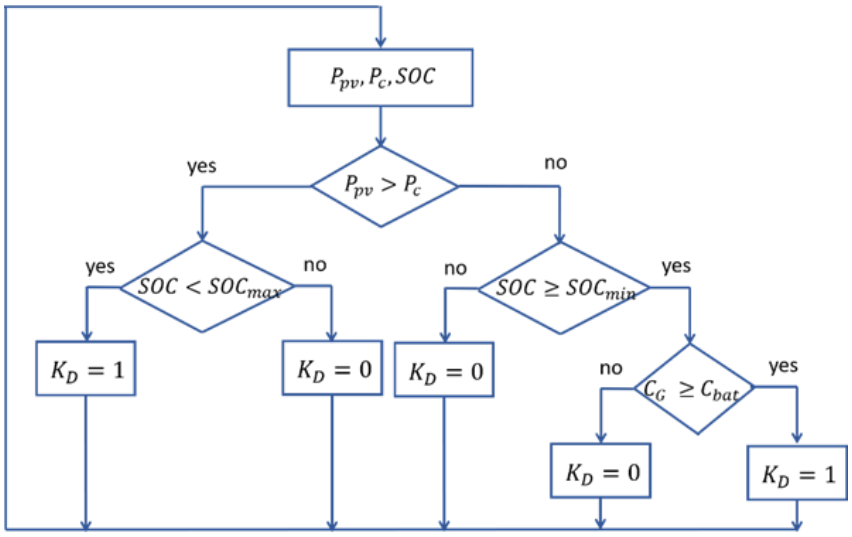

Figure 8. Flowchart of the strategy 2.

Hybrid energy storage system (HESS): as mentioned above, the HESS consists of a lithium-ion battery coupled with an SC. The strategy used to distribute energy between the battery and the SC is presented along with the simulation results. The energy management between the battery and SC is a filtering-based strategy.

To distribute the power between the battery and the SC, the filtering-based strategy was used as shown in Figure 9. The strategy based on filtering consists of distributing the power between the low and high frequency dynamics using a low pass filter [18]. The battery power P_{Bat} is the low frequency part of the P_{HESS} power, which is the total power of the hybrid storage system, while the high frequency part is the SCs power P_{SC}.

The battery power is the output of the low pass filter, and its value is directly related to the cut-off frequency of the low pass filter f_0 [19]. The value of this frequency is chosen so as to minimize the battery current. Figure 9 shows the filtering-based strategy principle.

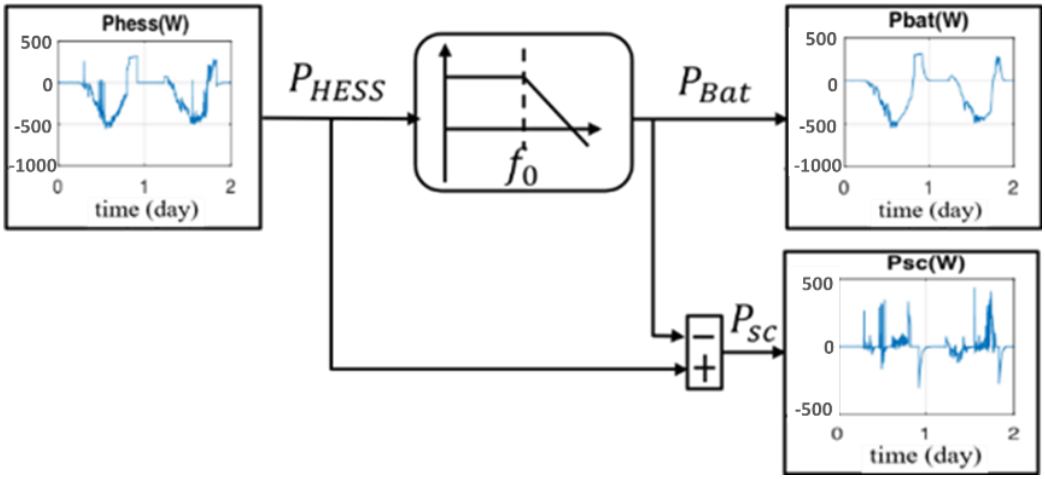

Figure 9. Filtering-based strategy.

3. Simulation Results

Simulations were carried out with each of the strategies defined above. The simulations last for 10 days with a time step of one minute. The generated power profile is a real profile of the UTC PV panel platform, from 1st to 10th June 2019. The load profile is a profile of the lighting consumption of a floor of the Laboratory for Analysis and Architecture of Systems (LAAS) building in Toulouse, from 1st to 10th June 2017. The load profile is assumed to be constant between 2017 and 2019. The temperature is constant at 25 °C for all simulations presented in this section. Two scenarios of *SOC* are considered: SOC_{max} = 100% and SOC_{max} = 80%.

Models for the components of the microgrid have been developed using the Matlab/Simulink software (Simulink models). Analytical models are based on common predefined HESS component's blocks selected on the Simulink interface, for which the internal and input parameters for aging and dynamic behavior models are calculated using analytical equations and routines implemented on the Matlab Workspace.

3.1. Comparison of Strategies 1 and 2 Regarding Battery Aging

The loss of battery capacity is much greater for strategy 1 as shown in Figure 10 (the values are presented in the following Table 2). In the first case, where the SOC_{max} is set to 100%, the lifetime is equal to 7 years for strategy 2 against 5.5 years for strategy 1, i.e., one and a half years longer (see Table 2). Other simulations were carried out with a maximum *SOC* of 80%. These simulation results show that the gap increases to 2.2 years when the SOC_{max} is set to 80%. The higher the *SOC*, the greater the capacity loss [20,21]. According to the model chosen in Equations (2)–(5), extreme temperatures (very cold or very hot) and high *SOCs* favor battery degradation.

In Figure 10, it can be seen that strategy 2 tends towards higher *SOCs* than strategy 1. This would normally lead to more aging for strategy 2. On the other hand, we observe a very high *SOC* recharge (from 70 to 100%) for strategy 1 on day 1 that does not exist in strategy 2. This recharge is reflected in the aging curves and is responsible for the main difference in aging between strategy 1 and strategy 2. These simulations were done with a temperature of 25 °C (northern France in June), with other more extreme scenarios, for example 0 or 40 °C, the differences between strategy 1 and 2 could become even more important.

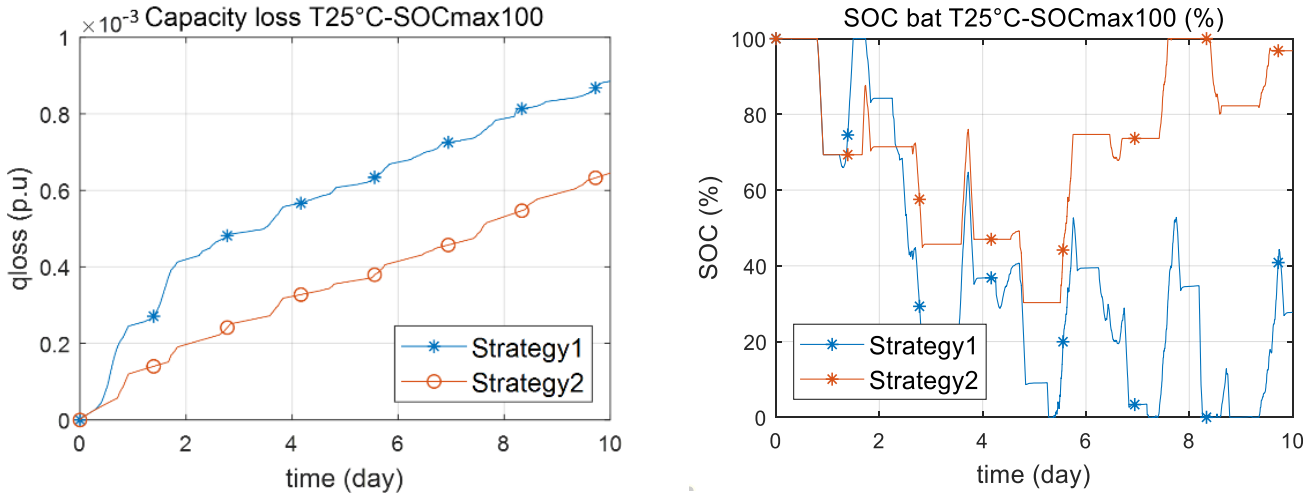

(**a**) (**b**)

Figure 10. Capacity loss (**a**) and SOC of the battery (**b**) for strategies 1 and 2.

Table 2. Total cost of strategies 1 and 2 for a 20-year microgrid project with SOC_{max} = 100 and T = 25 °C.

	Strategy 1	**Strategy 2**
qloss (p.u. × 10^{-4})	10	7.84
Battery life (years)	5.5	7
Total cost of energy purchased for 20 years (EUR)	720	2380
Number of battery replacements over 20 years	4	3
Battery cost over 10 years (EUR)	18,201	14,308
Total project cost over 10 years (EUR)	18,921	16,688

3.2. Techno-Economic Study

Table 2 above shows the total cost (battery price + cost of energy purchased from the utility grid) in a 20-year microgrid project. The total cost of energy purchased from the utility grid over a year is higher in strategy 2. This is due to the fact that strategy 2 favors the purchase of energy over the use of the battery (especially when the cost of grid energy is cheaper) to improve the lifetime of the battery. However, the total cost over the life of the project (here, 20 years), including the price of the batteries multiplied by the number of times they are replaced, for each strategy, means that strategy 2 becomes much cheaper. At the end of the project, strategy 2 will have cost EUR 16,688 compared to EUR 18,921 for strategy 1. The batteries are replaced three times in strategy 2 against four times in strategy 1. In conclusion, strategy 2 is much more advantageous than strategy 1. Considering the aging aspect in real-time management, this allowed the life of the batteries to be extended and the total cost of the installation to be reduced by reducing the cost of the batteries.

3.3. Simulation Results of the HESS

The total power of the HESS, P_{HESS}, the powers of battery P_{Bat}, and SCs P_{SC} are presented in Figure 11 below. One notes that the coupling between the battery and the SCs through filtering has resulted in a much smoother current at the battery. The HESS avoids applying high frequency currents directly to the battery. These currents are largely responsible for the premature aging of batteries.

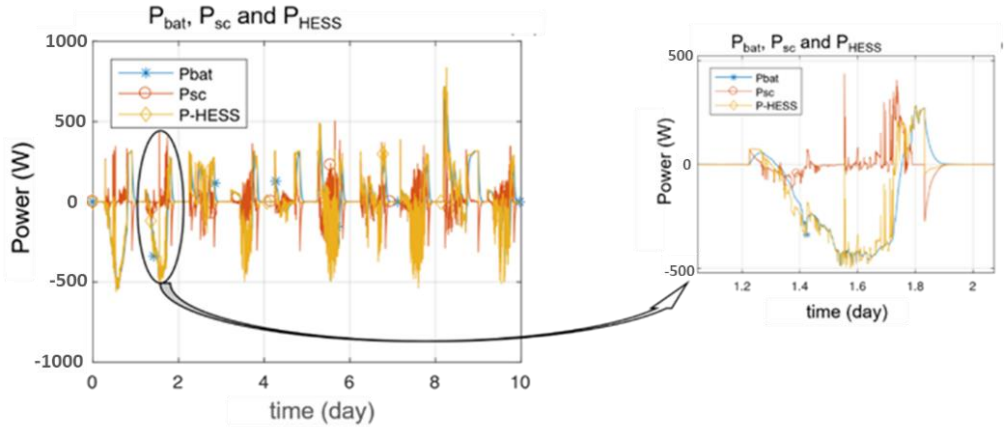

Figure 11. Total unfiltered HESS power, filtered SC, and battery power.

In Figure 12 below, it can be seen that filtering the current has a positive influence on the capacity loss of the battery.

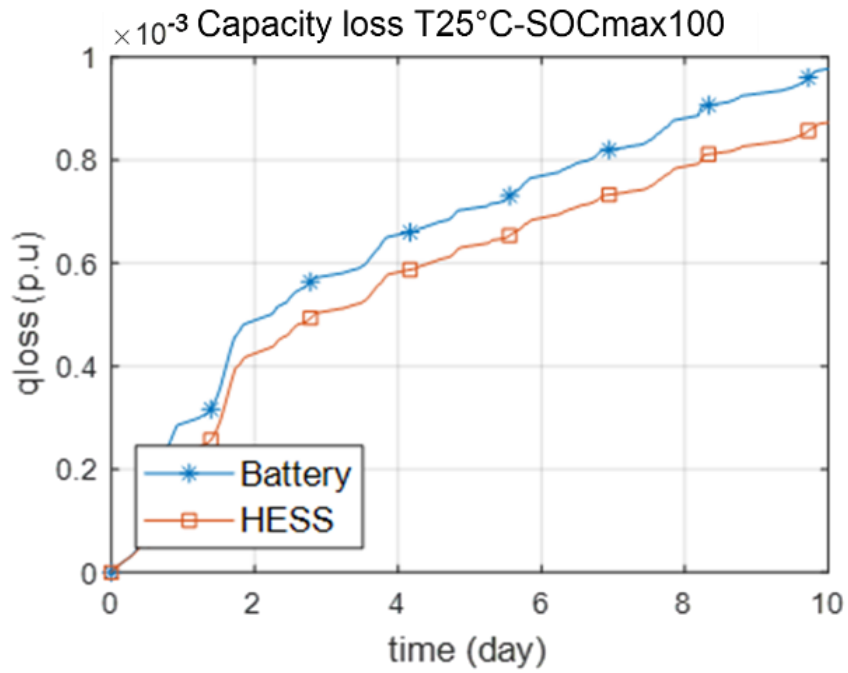

Figure 12. Battery capacity loss in HESS versus classical strategy 1.

The loss of battery capacity increased from 0.1% for 10 days of simulation with the battery alone to 0.085% with the hybrid storage system. This corresponds to a gain of 10 months in battery life. Figure 13 shows the capacitor *C* and *ESR* of the SCs. The capacity of the SCs lost over the 10 days simulation is 0.0119% corresponding to a theoretical lifetime (by extrapolation) of "34 years". This large value could be explained by the low values of currents flowing through the SCs. A comparative cost study is not performed in this section. This is one of the perspectives of this work.

3.4. Simulation Results under Extreme Temperature Conditions

The capacity loss at very low and very high temperatures can be estimated by the battery aging model presented in Section 2. In this section, the battery is decoupled from the supercapacitors and simulated under extreme temperature conditions (−20 °C, 0 °C, 45 °C, and 60 °C). The capacity loss under these conditions is compared to that obtained in simulation at a temperature of 25 °C. The simulation results are shown in Figure 14. At

45 °C and 60 °C, the capacity fade is higher than that at 25 °C. At 60 °C an accelerating effect of the temperature is clearly identified. After 10 days of simulation at this temperature, qloss has tripled compared to 25 °C. It can be concluded that high temperatures accelerate lithium-ion battery aging. On the other hand, at a low temperature (0 °C), the capacity loss is almost the same or even lower than that at 25 °C. This could be explained by the fact that the charge and discharge current is low (<C/10). Therefore, there is no formation of lithium plating at 0 °C. However, at −20 °C, there is a degradation of performance with a higher capacity loss than that at 25 °C.

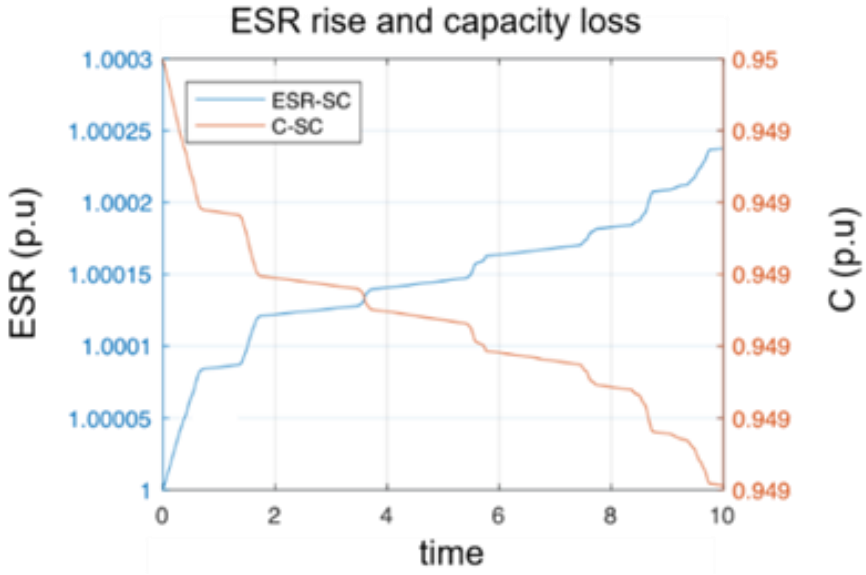

Figure 13. Capacity loss and ESR rise of the SCs.

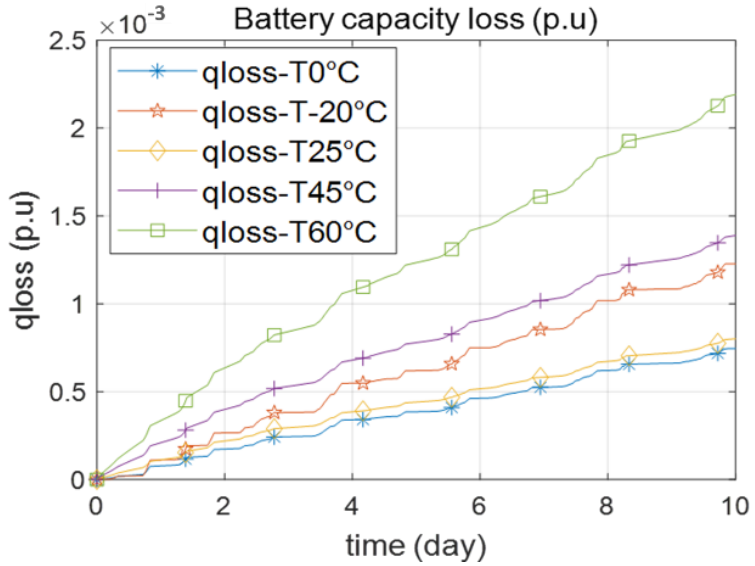

Figure 14. Battery capacity loss under extreme temperature conditions.

4. Conclusions and Perspectives

Strategies and scenarios for the batteries are presented either based on *SOC* limitation or hybrid association with SCs in order to extend their lifetime in microgrid operation, while in the meantime searching for a method of minimizing the installation costs. In the first part, the strategy consists of improving conventional energy management by considering battery aging. The results show that energy management allows us to extend

the lifetime of the batteries and to lower the costs of the microgrid project depending on the chosen strategy. In the second part, the battery is coupled with SCs. The filtering strategy is used to distribute the energy between the battery and the SCs. Results show that high frequency currents are eliminated and battery life is improved. The results obtained in this paper demonstrate the key role of the techno-economic approach and knowledge of the aging processes of storage devices for improving the energy management and global feedback costs of microgrids. In the future, other scenarios will be considered, such as longer simulations over time. The power performance degradation due to the battery aging will be considered. The SCs will be dimensioned to further the techno-economic study in the case of the hybrid energy storage system. This study would allow us to know if it is advantageous or not to couple the batteries with SCs. Finally, energy management will be improved through more elaborate optimization algorithms.

Author Contributions: Conceptualization, A.N., F.L., A.D.B., M.S. and E.R.-I.; methodology, A.N., F.L., A.D.B., M.S. and E.R.-I.; software, A.N., F.L., A.D.B. and E.R.-I.; validation, A.N., F.L., A.D.B., M.S. and E.R.-I.; formal analysis, A.N., F.L., A.D.B. and E.R.-I.; investigation, A.N., F.L., A.D.B., M.S. and E.R.-I.; resources, A.N., F.L., A.D.B. and E.R.-I.; data curation, A.N., F.L. A.D.B. and E.R.-I.; writing—original draft preparation, A.N.; writing—review and editing, F.L., A.D.B., M.S. and E.R.-I.; visualization, A.N., F.L., A.D.B., M.S. and E.R.-I.; supervision, F.L., A.D.B. and E.R.-I.; project administration, F.L., A.D.B., M.S. and E.R.-I.; funding acquisition, F.L., A.D.B. and M.S. All authors have read and agreed to the published version of the manuscript.

Funding: This research was funded by CNRS GDR SEEDS, grant Catelsemir and the APC was funded by Université de Technologie de Compiègne.

Institutional Review Board Statement: Not applicable.

Informed Consent Statement: Not applicable.

Data Availability Statement: Not applicable.

Conflicts of Interest: The authors declare no conflict of interest.

References

1. Bai, W.; Sechilariu, M.; Locment, F. DC Microgrid System Modeling and Simulation Based on a Specific Algorithm for Grid-Connected and Islanded Modes with Real-Time Demand-Side Management Optimization. *Appl. Sci.* **2020**, *10*, 2544. [CrossRef]
2. Østergaard, P.A.; Sperling, K. Towards Sustainable Energy Planning and Management. *Int. J. Sustain. Energy Plan. Manag.* **2014**, *1*, 1–6. [CrossRef]
3. Ribó-Pérez, D.; Bastida-Molina, P.; Gómez-Navarro, T.; Hurtado-Pérez, E. Hybrid assessment for a hybrid microgrid: A novel methodology to critically analyse generation technologies for hybrid microgrids. *Renew. Energy* **2020**, *157*, 874–887. [CrossRef]
4. Ndiaye, A.; Locment, F.; De Bernardinis, A.; Sechilariu, M.; Redondo-Iglesias, E. First approach for a techno-economic analysis of storage components used for improving energy management strategies in microgrids. In Proceedings of the 16th Conference on Sustainable Development of Energy Water and Environment Systems—SDEWES, Dubrovnik, Croatia, 10–15 October 2021.
5. Lee, J.-W.; Kim, M.-K.; Kim, H.-J. A Multi-Agent Based Optimization Model for Microgrid Operation with Hybrid Method Using Game Theory Strategy. *Energies* **2021**, *14*, 603. [CrossRef]
6. Al-Sakkaf, S.; Kassas, M.; Khalid, M.; Abido, M.A. An Energy Management System for Residential Autonomous DC Microgrid Using Optimized Fuzzy Logic Controller Considering Economic Dispatch. *Energies* **2019**, *12*, 1457. [CrossRef]
7. Hussain, A.; Bui, V.-H.; Kim, H.-M. Fuzzy Logic-Based Operation of Battery Energy Storage Systems (BESSs) for Enhancing the Resiliency of Hybrid Microgrids. *Energies* **2017**, *10*, 271. [CrossRef]
8. Paccha-Herrera, E.; Calderón-Muñoz, W.R.; Orchard, M.; Jaramillo, F.; Medjaher, K. Thermal Modeling Approaches for a $LiCoO_2$ Lithium-ion Battery—A Comparative Study with Experimental Validation. *Batteries* **2020**, *6*, 40. [CrossRef]
9. Damay, N.; Forgez, C.; Bichat, M.-P.; Friedrich, G. Thermal modeling of large prismatic LiFePO 4/graphite battery. Coupled thermal and heat generation models for characterization and simulation. *J. Power Sources* **2015**, *283*, 37–45. [CrossRef]
10. German, R.; Shili, S.; Desreveaux, A.; Sari, A.; Venet, P.; Bouscayrol, A. Dynamical Coupling of a Battery Electro-Thermal Model and the Traction Model of an EV for Driving Range Simulation. *IEEE Trans. Veh. Technol.* **2019**, *69*, 328–337. [CrossRef]
11. Redondo-Iglesias, E.; Venet, P.; Pelissier, S. Global Model for Self-Discharge and Capacity Fade in Lithium-Ion Batteries Based on the Generalized Eyring Relationship. *IEEE Trans. Veh. Technol.* **2017**, *67*, 104–113. [CrossRef]
12. Kovaltchouk, T.; Multon, B.; Ben Ahmed, H.; Aubry, J.; Venet, P. Enhanced Aging Model for Supercapacitors Taking Into Account Power Cycling: Application to the Sizing of an Energy Storage System in a Direct Wave Energy Converter. *IEEE Trans. Ind. Appl.* **2014**, *51*, 2405–2414. [CrossRef]

13. De Bernardinis, A.; Reynaud, R.; Yakam, C.B.; Chabrak, Z.; Ben Ahmed, H.; Lallemand, R.; Kauv, J. Supercapacitors Aging Study: Models Theoretical Analysis and Attempt to Physical Correlation related to Applied Cycles for Transport Application. In Proceedings of the 2018 International Conference on Applied and Theoretical Electricity (ICATE), Craiova, Romania, 4–6 October 2018; pp. 1–8. [CrossRef]
14. Berrueta, A.; Martín, I.S.; Hernández, A.; Ursúa, A.; Sanchis, P. Electro-thermal modelling of a supercapacitor and experimental validation. *J. Power Sources* **2014**, *259*, 154–165. [CrossRef]
15. BCAP3000 P270 K04 Maxwell Technologies | Mouser. Mouser Electronics. Available online: https://www.mouser.fr/datasheet/2/257/Maxwell_K2Series_DS_1015370-4-1179730.pdf (accessed on 3 January 2022).
16. German, R.; Venet, P.; Sari, A.; Briat, O.; Vinassa, J.-M. Improved Supercapacitor Floating Ageing Interpretation Through Multipore Impedance Model Parameters Evolution. *IEEE Trans. Power Electron.* **2013**, *29*, 3669–3678. [CrossRef]
17. Sechilariu, M.; Locment, F.; Wang, B. Photovoltaic Electricity for Sustainable Building. Efficiency and Energy Cost Reduction for Isolated DC Microgrid. *Energies* **2015**, *8*, 7945–7967. [CrossRef]
18. Mutarraf, M.U.; Terriche, Y.; Niazi, K.A.K.; Khan, F.; Vasquez, J.C.; Guerrero, J.M. Control of Hybrid Diesel/PV/Battery/Ultra-Capacitor Systems for Future Shipboard Microgrids. *Energies* **2019**, *12*, 3460. [CrossRef]
19. Castaings, A.; Lhomme, W.; Trigui, R.; Bouscayrol, A. Comparison of energy management strategies of a battery/supercapacitors system for electric vehicle under real-time constraints. *Appl. Energy* **2016**, *163*, 190–200. [CrossRef]
20. Waldmann, T.; Kasper, M.; Wohlfahrt-Mehrens, M. Optimization of Charging Strategy by Prevention of Lithium Deposition on Anodes in high-energy Lithium-ion Batteries—Electrochemical Experiments. *Electrochim. Acta* **2015**, *178*, 525–532. [CrossRef]
21. Gao, Y.; Jiang, J.; Zhang, C.; Zhang, W.; Jiang, Y. Aging mechanisms under different state-of-charge ranges and the multi-indicators system of state-of-health for lithium-ion battery with Li(NiMnCo)O_2 cathode. *J. Power Sources* **2018**, *400*, 641–651. [CrossRef]